

# A NEW AUTOMATIC DETECTION APPROACH FOR HEPATOCELLULAR CARCINOMA USING $^{11}\text{C}$ -ACETATE POSITRON EMISSION TOMOGRAPHY

Sirong Chen<sup>1</sup>, Longkin Wong<sup>1</sup>, Dagan Feng<sup>1,2</sup>

1. Center for Multimedia Signal processing, Dept of Electronic and Information Engineering, Hong Kong Polytechnic University, Hong Kong.
2. Biomedical and multimedia information technology Group, School of Information Technologies, The University of Sydney, Australia.

Email address: Sirong Chen: [ensrchen@eie.polyu.edu.hk](mailto:ensrchen@eie.polyu.edu.hk)  
Longkin Wong: [00059788d@polyu.edu.hk](mailto:00059788d@polyu.edu.hk)  
Dagan Feng: [enfeng@polyu.edu.hk](mailto:enfeng@polyu.edu.hk)

**ABSTRACT:** Functional imaging techniques such as Positron Emission Tomography (PET) has the potential for early diagnosis of malignant tumors. However, 40-50% of Hepatocellular Carcinoma (HCC), a common malignancy worldwide, can hardly be detected by the widely used  $^{18}\text{F}$ -2-fluoro-2-deoxy-D-glucose (FDG) PET.  $^{11}\text{C}$ -acetate PET has recently been found effective for detecting HCC. To perform quantitative analysis to obtain the diagnosis information, regions of interest (ROIs) are needed to be extracted. Manual placement of ROIs is subject to operator's skill and time-consuming. Furthermore, the small sizes of some ROIs make the task even more difficult. In this paper, we propose an approach to segment the dynamic  $^{11}\text{C}$ -acetate PET liver images automatically. The curves extracted from some segmented ROIs are then fitted to the presented  $^{11}\text{C}$ -acetate liver model. Finally, the parameter K, which has been validated as an indicator for detecting HCC, can be calculated.

**Keywords:** Cluster analysis, Segmentation, Hepatocellular Carcinoma (HCC), Positron Emission Tomography (PET), parameter K.

## INTRODUCTION

Hepatocellular Carcinoma (HCC) is a common cause of cancer deaths. However, most cases of HCC are discovered late and less than 10% are cured with surgical resection. Overall 5-year survival rate is less than 5% [1], [2]. Dynamic Positron Emission Tomography (PET) has been extensively used to quantify *in vivo* the physiological and biochemical processes in humans, which could achieve early diagnosis of malignant tumors. However, 40-50% of HCC couldn't be detected by the widely used  $^{18}\text{F}$ -2-fluoro-2-deoxy-D-glucose (FDG) PET. It is clearly not acceptable in countries where this tumor is one of the top 3 causes of cancer deaths.  $^{11}\text{C}$ -acetate PET has recently been conducted and found to be a complementary

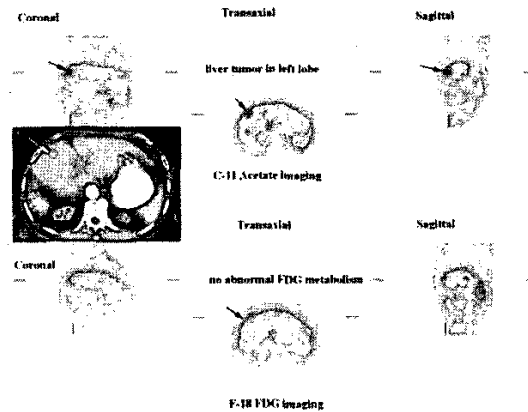


Figure 1: CT demonstrates a hypervascular lesion in the L lobe of liver (status post R lobectomy for HCC); FDG imaging shows no abnormal FDG uptake;  $^{11}\text{C}$ -acetate imaging shows increased metabolism.

tracer to FDG in PET imaging of HCC [3] [4]. Fig. 1 demonstrates a case of recurrent HCC in the left lobe of liver after right lobectomy. CT shows hypervascularity within the tumor. FDG-PET imaging shows no abnormal FDG uptake by the tumor, whereas  $^{11}\text{C}$ -acetate PET imaging shows increased metabolism.

To get a better understanding of the characteristics of  $^{11}\text{C}$ -acetate in HCC liver images, quantitative dynamic modeling has been conducted [4]. The tracer time-activity curve in blood (BTAC) is used as the input function in the kinetic model. BTAC is usually represented by a sequence of arterial or arterialized blood samples [5], [6], which is in general very invasive and requires extra personnel and processing time. Moreover, the liver has a dual source of blood supply: the hepatic artery (HA) and the portal vein (PV), it is highly invasive and virtually impossible in

clinical settings to count the radioactivity of the portal venous blood by direct catheterization and sampling. Therefore, regions-of-interest (ROIs) delineation of HA and PV is required from the dynamic PET images. However, PET cannot provide precise anatomic localization due to its relatively poor spatial resolution and high noise level. Manual placement of ROIs is subject to operator's skill and lacks of reproducibility. It is also time consuming [7]. Furthermore, the sizes of both HA and PV are very small, which makes the delineation even more difficult. Therefore, automatic segmentation should be our preliminary step for enhancement of visualization and ROI analysis. In addition, automatic segmentation could provide consistent and reproducible results and an overall reduction in time for data analysis [7].

Clustering algorithms achieve region segmentation by partitioning the image into sets of clusters of pixels that have strong similarity in the feature space [8]. This approach has been used with some success in segmentation of PET images. For dynamic PET images, each pixel of a slice could be represented by a time-activity curve (TAC). In our study, cluster analysis is used to segment the dynamic PET images by merging a number of TACs according to their shapes and magnitudes into a small number of distinct characteristic classes so that the TACs within a cluster showing the greatest similarity to each other but are dissimilar to those extracted from other clusters [7]. However, for liver study, the tracer arriving at the PV is delayed and dispersed in comparison with that of the HA [9], which makes its activity in PV similar to that in the normal liver tissue. If the number of clusters is insufficient, the region of PV would be merged into the surrounding hepatic parenchyma and cannot be distinguishable; if the number of clusters is adequate to identify the PV, several "meaningless" clusters would appear. A two-step segmentation method based on clustering algorithm and with the combination of spatial and temporal information provided by the dynamic PET liver images, is proposed as well in this paper.

A three-compartment four-parameter (4P) kinetic model for evaluation of  $^{11}\text{C}$ -acetate metabolism in liver is then adopted to fit the curves of the segmented regions of HCC and non-tumor liver tissue. The physiological parameter  $K_1$ , which is defined as  $K_1 \cdot k_3 / (k_2 + k_3)$ , is introduced as the indicator for the detection of HCC.

## METHODS

### Data Acquisition

The two-step segmentation method has been applied to clinical dynamic  $^{11}\text{C}$ -acetate PET liver images. An ECAT-

EXACT 47 PET scanner (CTI/Siemens, Inc., TN, USA) is used for 2D dynamic image acquisition. Full sets of dynamic data in one single position, covering the liver dome and apical half of the left ventricle to the inferior part of liver, are obtained for 10 min immediately following bolus IV injection of  $^{11}\text{C}$ -acetate. Sampling acquisition sequence is as follows: 4 sec frames x 10, 10 sec frames x 8, 30 sec frames x 2, 60 sec frames x 3 and 120 sec frames x 2, a total of 25 frames.

### Segmentation Scheme

Our aims of the segmentation are to differentiate image pixels of the pathological regions: HCC, from other liver masses, at the same time extract the specific anatomic structures: HA and PV from the dynamic  $^{11}\text{C}$ -acetate PET liver images. The segmentation is performed independently on each slice. The basic idea of the segmentation method is to utilize clustering algorithm to merge all the pixels' TACs according to their shapes and magnitudes into a small number of distinct characteristic clusters. The cluster centroid is the average of all pixels' TACs in the cluster. Assume that there are totally  $n$  pixels' TACs of  $p$  time frames in the dynamic PET data and  $m$  distinct characteristic curves ( $m \ll n$ ). Each pixel's TAC belongs to only one of the  $m$  curves. The clustering algorithm can segment the dynamic PET data into  $m$  curves automatically based on a least squares distance  $D$

$$D\{z_i, \mu_j\} = \sum_{j=1}^m \sum_{i=1}^n \|z_i - \mu_j\|^2 \quad (1)$$

where  $z_i$  is the  $i$ th pixel's TAC in the PET data;  $\mu_j$  is the centroid of  $j$ th cluster [7]. Each pixel's TAC is allocated to its nearest cluster centroid according to

$$\|z_i - \mu_i\|^2 < \|z_i - \mu_j\|^2 \quad i, j = 1, 2, \dots, m, i \neq j \quad (2)$$

where  $z_i$  is the  $i$ th pixel's TAC in the PET data;  $\mu_i$  and  $\mu_j$  are the  $i$ th and  $j$ th cluster centroid respectively. The cluster centroids will be updated by averaging all pixels' TACs in the cluster after each round of allocation based on (2) to minimize  $D$ . Then, the  $n$  TACs are needed to be reallocated according to the new cluster centroids. The allocation and updating iteration wouldn't cease until no TAC is needed to be reallocated from a cluster to another.

In the first step of the segmentation, we aim to extract the PV, which has very similar characteristic with the surrounding liver tissue. An option to cluster the similar objects is to increase the number of clusters. Therefore, we perform the segmentation on the dynamic  $^{11}\text{C}$ -acetate PET liver images with a relatively large number of clusters  $k$  by using the above-mentioned method.  $k$  is assigned to a value that the PV can be distinguished from its surroundings. The segmented PV may be validated by the spatial information: its invariable anatomical position

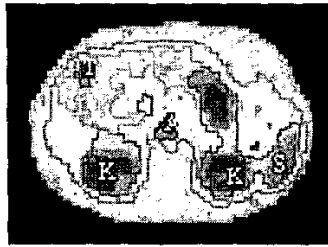


Figure 2: The segmentation result of one slice of clinical dynamic  $^{11}\text{C}$ -acetate PET liver images using cluster analysis. A = HA, K = kidney, L = liver, S = spleen, T = HCC.

being posterior to the pancreatic head that shows the most intense physiological uptake of  $^{11}\text{C}$ -acetate, or by direct reference to the CT images. Since PV couldn't be recognized clearly on the  $^{11}\text{C}$ -acetate PET liver images, contrast enhancement techniques are conducted to help validate the segmentation result. After the first round of segmentation, the PV would be identified; all the clusters will be labeled and isolated. The remaining clusters are then put into a queue. In this stage, the PET images are over-segmented.

In the first step of segmentation, each cluster has equal significance to the result, however it is unnecessary to retain all the other clusters and some clusters are even "meaningless". Therefore, in the second step, cluster analysis is again performed, but only to the pixels belong to the clusters inside the queue. This time, the number of clusters is set to be 8 as *a priori* according to [7]. Since the cluster of the PV is labeled and isolated, it won't affect the result of the second step segmentation. In addition, it will not be interfered. Finally, 9 clusters are obtained and all the ROIs needed for the quantitative analysis of the  $^{11}\text{C}$ -acetate PET liver images could be extracted.

#### Parameter estimation

The results of our previous validation study show that the three-compartment 4P kinetic model (without  $k_4$ ), including a hepatic blood volume (HBV) term, is suitable for describing  $^{11}\text{C}$ -acetate kinetics in liver [4]. The ROIs' curves of HCC and non-tumor liver tissue obtained by our segmentation are fitted to the model. Both the extracted curves of HA and PV would be used as the model inputs. Since the radioactivity spillover from the surrounding tissue to the PV is significant, especially at the later part of the study when the tracer concentration in tissue is much higher than that in the PV. Munk et al. [9] suggested that the difference between the two blood TACs is most pronounced around the peak and immediately after the bolus injection. After some time they are virtually identical. Therefore, the last five measurements of the TACs of the PV from the dynamic PET liver images are

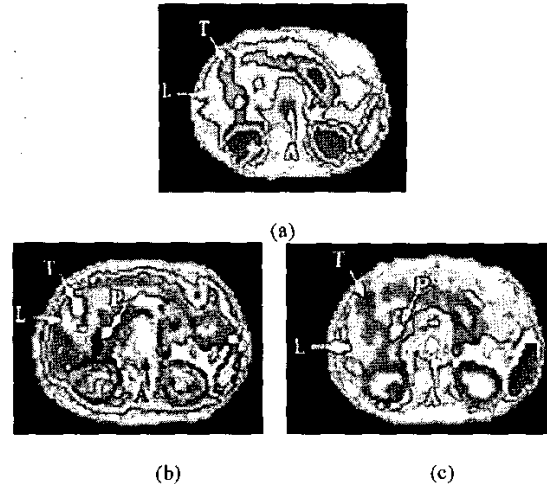


Figure 3. (a) The segmentation result of another slice of clinical dynamic  $^{11}\text{C}$ -acetate PET images using cluster analysis directly; (b) result of our first step segmentation; (c) final result of our two-step segmentation. A = HA, L = liver, P = PV, T = HCC.

replaced by the HA data in this study. Preliminary studies [4] show that the forward clearance  $K=K_1*k_3/(k_2+k_3)$  of the non-FDG-avid type of HCC is significantly higher than that of normal tissue ( $p < 0.05$ ), so the parameter K could be used to detect HCC. When  $k_4$  is assumed to be zero, K value can be estimated by Patlak analysis [10]. The ratio of  $c_T(t)$  (tracer concentration in tissue) and the vascular input function  $c_b(t)$  can be calculated by

$$\frac{c_T(t)}{c_b(t)} = \frac{K}{c_b(t)} \int_0^t c_b(\tau) d\tau + \frac{K_1 k_2}{(k_2 + k_3)^2} + HBV \quad (3)$$

$$K = \frac{K_1 k_3}{k_2 + k_3} \quad (4)$$

The data points chosen are within the period from 1.5 min to 10 min.

## RESULTS AND CONCLUSION

Fig. 2 shows a typical segmentation result of one slice of clinical dynamic  $^{11}\text{C}$ -acetate PET liver images using cluster analysis. As seen in Fig. 2, except PV, other anatomical structures such as HA, HCC, liver, kidney, spleen, etc, could be recognized clearly. The number of clusters used is 8. Fig. 3 demonstrates our proposed two-step segmentation results of another slice of clinical dynamic  $^{11}\text{C}$ -acetate PET liver images in comparison with the segmentation results by using cluster analysis directly. From Fig. 3a, it could be seen that the liver, HA, HCC could be identified, but the PV are merged into the surrounding hepatic parenchyma. The results are also of 8 clusters. 24 clusters are adopted in our first step

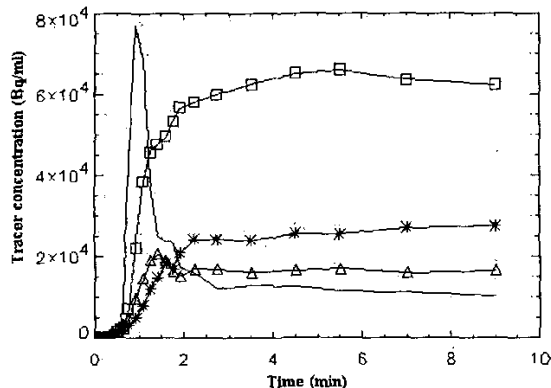


Figure 4. TACs extracted from the results of the proposed two-step segmentation method. Pure solid line stands for the curve of HA; solid line marked by triangle is for the PV, square for HCC and asterisk for the non-tumor liver tissue.

segmentation whose result is show in Fig. 3b. The PV can be differentiated clearly, however, some anatomical structures are distorted and some clusters are even "meaningless" compared to Fig. 3a. Fig. 3c illustrates the result after our two-step segmentation using 9 clusters totally. The PV still could be seen; other ROIs in Fig. 3a also appear in Fig. 3c and their respective locations and shapes are nearly unchanged when compared with Fig. 3a. Therefore, all the ROIs needed for the quantitative study could be extracted. Fig. 4 shows the TACs of the clusters of HA, PV, HCC and non-tumor liver tissue obtained from the segmentation results. The extracted HCC and non-tumor liver tissue curves are then fitted to the three-compartment 4P model. The linear Patlak analysis is used to estimate the parameter  $K$ , which is formulated by  $K_1 * k_3 / (k_2 + k_3)$ . Results are given as the estimated value  $\pm$  standard deviation (SD). The estimated  $K$  value of the non-tumor liver tissue is  $0.174 \pm 0.025$  ml/min/ml; whereas the estimated  $K$  value of HCC is  $0.355 \pm 0.061$  ml/min/ml. The functional parameter  $K$  did show significant difference between the non-FDG-avid type of HCC and the non-tumor liver parenchyma. Therefore, parametric image of the estimated  $K$  value generated from the dynamic  $^{11}\text{C}$ -acetate PET liver images could be used for HCC detection.

The approach presented in this paper could segment the dynamic  $^{11}\text{C}$ -acetate PET liver images automatically. All the ROIs for the quantitative study of  $^{11}\text{C}$ -acetate liver characteristics could be obtained by using the proposed two-step segmentation method. This segmentation may also be useful as a preprocessing step before fast generation of parametric images. Parametric image of the physiological parameter  $K$  could characterize the regional consumption of acetate by HCC and non-tumor tissue of

the liver, which could be a powerful tool to detect HCC automatically. Additionally, the proposed two-step segmentation method may open a window for automatic detection of other PET studies.

#### ACKNOWLEDGEMENT

This work is supported by the studentship of the Hong Kong Polytechnic University, partially by UGC and ARC grants. The authors would also like to express their sincere gratitude to Dr. Chilai Ho, director of the Dept. of Nuclear Medicine & PET, Hong Kong Sanatorium and Hospital, for his kindly support.

#### REFERENCES

- [1] T. Tsuzuki, A. Sugioka, M. Ueda, "Hepatic resection for hepatocellular carcinoma", *Surgery*, vol. 107, pp. 511, 1990.
- [2] K. T. Watkins, S. A. Curley, "Liver and bile ducts", In Abeloff MD, Armitage JO, Lichter AS, Niederhuber JE (eds), *Clinical oncology*, 2nd Ed, Science Press, Harcourt Asia, Churchill Livingstone, pp. 1681, 2000.
- [3] C. Ho, C. Yu, D. Yeung, " $^{11}\text{C}$ -acetate PET imaging in Hepatocellular carcinoma and other liver masses", *J. Nucl. Med.*, (in press).
- [4] S. Chen, C. Ho, D. Feng, Zheru Chi, "Tracer Kinetic Modeling of  $^{11}\text{C}$ -acetate Applied in the Liver with Positron Emission Tomography", *IEEE Transactions on Medical Imaging*, accepted, Sep. 2002.
- [5] S. C. Huang, M. E. Phelps, E. J. Hoffman, K. Sideris, C. J. Selin, and D. E. Kuhl, "Noninvasive determination of local cerebral metabolic rate of glucose in man", *Amer. J. Physiol.*, vol. 238, pp. E69-E82, 1980.
- [6] M. E. Phelps, S. C. Huang, E. J. Hoffman, C. Selin, L. Sokoloff and D. E. Kuhl, "Tomographic measurement of local cerebral glucose metabolic rate in humans with (F-18) 2-Fluoro-2-Deoxy-D-Glucose: validation of method", *Ann. Neurol.*, vol. 6, pp. 371-388, 1979.
- [7] K. P. Wong, D. Feng, S. R. Meikle, M. J. Fulham, "Segmentation of Dynamic PET Images Using Cluster Analysis", *IEEE Trans. Nucl. Sci.*, vol. 49, no. 1, pp. 200-207, Feb. 2002.
- [8] Handbook of Medical Imaging processing and analysis, editor-in-chief Isaac N. Bankman, Academic press, San Diego, USA, 2000. ISBN: 0-12-077790-8.
- [9] O. L. Munk, L. Bass, K. Roelsgaard, D. Bender, S. B. Hansen, and S. Keiding, "Liver kinetics of glucose analogs measured in pigs by PET: importance of dual-input blood sampling", *J. Nucl. Med.*, vol. 42, no. 5, pp. 795-801, 2001.
- [10] C. S. Patlak, R. G. Blasberg, and J. D. Fenstermacher, "Graphical evaluation of blood-to-brain transfer constants from multiple-time uptake data", *J. Cereb. Blood Flow Metab.*, vol. 3, pp. 1-7, 1983.